Global Hypomethylation of Genomic DNA in Cancer-Associated Myofibroblasts

Le Jiang,[1] Tamas A. Gonda,[2] Mary V. Gamble,[3] Martha Salas,[1] Venkatraman Seshan,[4] Shuiping Tu,[2] William S. Twaddell,[5] Peter Hegyi,[6] Gyorgy Lazar,[6] Islay Steele,[7] Andrea Varro,[7] Timothy C. Wang,[2] and Benjamin Tycko[1,5]

[1]Institute for Cancer Genetics and Departments of [2]Medicine, [3]Environmental Health Sciences, [4]Biostatistics, and [5]Pathology, Columbia University, New York, New York; [6]Departments of Medicine and Surgery, University of Szeged, Szeged, Hungary; and [7]Physiological Laboratory, School of Biomedical Sciences, University of Liverpool, Liverpool, United Kingdom

Abstract

Global hypomethylation has long been recognized as a feature of the malignant epithelial component in human carcinomas. Here we show evidence for this same type of epigenetic alteration in cancer-associated stromal myofibroblasts. We used methylation-sensitive SNP array analysis (MSNP) to profile DNA methylation in early-passage cultures of stromal myofibroblasts isolated from human gastric cancers. The MSNP data indicated widespread hypomethylation in these cells, with rare focal gains of methylation, conclusions that were independently validated by bisulfite sequencing and by a methylation-sensitive cytosine incorporation assay. Immunohistochemistry with anti–5-methylcytosine (anti–5-methyl-C) in a series of gastrectomy specimens showed frequent loss of methylation in nuclei of both the malignant epithelial cells and α-smooth muscle actin (ASMA)–positive stromal myofibroblasts of both intestinal-type and diffuse carcinomas. We confirmed this phenomenon and established its onset at the stage of noninvasive dysplastic lesions by immunohistochemistry for anti–5-methyl-C in a transgenic mouse model of multistage gastric carcinogenesis. These findings indicate similar general classes of epigenetic alterations in carcinoma cells and their accompanying reactive stromal cells and add to accumulating evidence for biological differences between normal and cancer-associated myofibroblasts. [Cancer Res 2008;68(23):9900–8]

Introduction

Stromal cells are increasingly recognized as influencing the biological behavior of human cancers. Among the various stromal cell types, much recent research has focused on cancer-associated fibroblasts, which often acquire a myofibroblast phenotype, defined by strong expression of α-smooth muscle actin (ASMA). The presence of such reactive cells originally suggested the classic concept of cancer as a nonhealing wound (1), and a number of observations, including clinicopathologic correlations and functional studies, have more recently implicated these cells as actively contributing to cancer growth, invasion, and metastasis (2–6). In parallel with this work, several laboratories have recently extended the fields of cancer genetics and epigenetics to examination of stromal cells, and there is now evidence, albeit in part controversial, for point mutations, loss of heterozygosity (LOH), and both losses and gains of DNA methylation at specific loci in cancer-associated stroma (7–15). Here we describe global DNA hypomethylation and focal gain of DNA methylation, without gross chromosomal instability, in stromal myofibroblasts of gastric carcinomas.

Materials and Methods

Cells and tissues. Tissue from human gastrectomy specimens was obtained immediately after resection from the Department of Surgery, University of Szeged, Szeged, Hungary. The study was approved by the Ethical Committee of that institution (2069/2006). Materials were taken from the cancer and from macroscopically normal gastric corpus mucosa resected at least 5 cm from the tumor margin. Both normal and cancer samples were confirmed by histopathology. Samples from the resected tissues were placed in ice-cold calcium and magnesium-free HBSS within 5 min. Myofibroblasts were prepared as reported previously (16). Briefly, gastrectomy tissues were transferred on ice immediately to the laboratory. The tissues were washed multiple times in calcium- and magnesium-free HBSS and were afterward incubated with 1 mmol/L DTT (Sigma) for 15 min, followed by six sequential 30-min incubations in 1 mmol/L EDTA while gassing with 95% O_2/5% CO_2 in a shaking water bath. The primary cultures were initially maintained in RPMI 1640 containing 10% FCS, which was changed to DMEM after 20 to 25 d of culture. The myofibroblasts were passaged a maximum of three to four times to accumulate sufficient early-passage material for these experiments. In two cases, DNA was isolated from myofibroblasts, both after three and six passages, to assess the effect of passage number on DNA methylation. Myofibroblasts were stained for ASMA and vimentin from each preparation to monitor purity; preparations with >1% ASMA- and vimentin-negative cells were rejected. DNA was isolated using QIAamp DNA mini kit (Qiagen). Formalin-fixed paraffin-embedded and frozen sections of primary gastric carcinomas and adjacent gastric tissue as well as sections of benign gastric ulcer specimens were obtained from the Molecular Pathology Shared Resource of the Herbert Irving Comprehensive Cancer Center at Columbia University. All tissues were obtained as anonymous specimens, with the pathologic diagnosis but without patient identifiers. Formalin-fixed paraffin-embedded tissue was also obtained from interleukin 1β (IL-1β) transgenic mice. In these animals, IL-1β cDNA is expressed from the murine H/K-ATPAse promoter (17). These animals developed gastric epithelial dysplasia 6 to 9 mo after infection, and 30% of the male mice developed carcinoma *in situ* in the subsequent 6 to 8 mo.[8]

Methylation-sensitive SNP array analysis probes. The preparation of methylation-sensitive SNP array analysis (MSNP) probes was essentially as previously described (18, 19). Genomic DNA samples (250 ng) were first

Note: Supplementary data for this article are available at Cancer Research Online (http://cancerres.aacrjournals.org/).

L. Jiang and T.A. Gonda contributed equally to this work.

Requests for reprints: Benjamin Tycko, Columbia University, 1130 St. Nicholas Avenue, New York, NY 10032. Phone: 212-305-1149; Fax: 212-305-5498; E-mail: bt12@columbia.edu.

doi:10.1158/0008-5472.CAN-08-1319

[8] Manuscript in preparation.

digested in the appropriate low-salt buffer with 10 units of *Hpa*II or *Msp*I or mock digested (no enzyme) in a volume of 12 μL for 3 h. The buffer was then adjusted to higher salt concentration by adding 3.2 μL of 10× buffer 3 (New England Biolabs); 10 units of *Sty*I restriction enzyme was added; and digestion was continued for a further 3 h. The enzymes were heat inactivated at 65°C for 20 min and the digested DNA samples (*Sty*I alone, preparation in duplicate; *Sty*I + *Hpa*II, preparation in duplicate; *Sty*I + *Msp*I, single preparation; for a total of five probe preparations per original DNA sample) were brought forward for linker ligation, amplification by PCR with linker primers, and fragmentation and labeling with biotin as specified in the Affymetrix protocol. The resulting probes were hybridized to 250K *Sty*I SNP arrays (five arrays per biological sample), washed, and scanned according to the Affymetrix protocol.

MSNP data analysis. The MSNP data (.cel files) were analyzed in dChip [9] (20) by normalization, model-based expression (perfect match/mismatch and perfect match-only methods gave similar results in this data set), and chromosome analysis. This sequential procedure in dChip is identical to that which is typically used for assessing DNA copy number. We first analyzed the *Sty*I-only array data from the myofibroblasts samples for possible changes in DNA copy number, loading these files together with SNP array data from four normal peripheral blood controls, and after finding no detectable chromosomal or subchromosomal gains or losses in the sample information file, we next assigned a numerical ploidy of "2" to all of the *Sty*I-only arrays from the myofibroblasts, leaving the numerical ploidy field blank for the *Sty*I + *Hpa*II and *Sty*I + *Msp*I arrays. This strategy allowed us to visualize, using the chromosome view in dChip, the methylation status of *Hpa*II sites flanking a given SNP-tagged locus as reduced signal intensity in the *Sty*I + *Hpa*II representations compared with the *Sty*I-only representations. The *Sty*I + *Msp*I representations allowed us to determine the reliability of the class 2 SNPs, with greatest reliability indicated by the strongest and most consistent reduction in signal intensity in the *Sty*I + *Msp*I representations compared with the *Sty*I-only representations. To quantitate the degree of methylation at each class 2 SNP, we derived a methylation index by carrying out normalization and model-based expression in dChip, exporting the resulting SNP intensity values, subtracting the average *Sty*I + *Msp*I value at each SNP as background, and then calculating the percent preservation of intensity in *Sty*I + *Hpa*II compared with *Sty*I only.

Bisulfite sequencing. Genomic DNA (1 μg) was bisulfite converted using the CpGenome universal DNA modification kit (Millipore) according to the instructions of the manufacturer. Sequences including or adjacent to the index SNPs were amplified by PCR using primers designed with the MethPrimer program (21).[10] PCR conditions, primer sequences, and corresponding unconverted genomic sequences were as follows: SNP_A-2105245 (rs10259620; HOXA9) bis-For, TGAGAGTGGTTTTTTTATTGTTATTG; bis-Rev, CCCCAATTTTACCTCTAACTAACTTT (unconverted sequences For, TGAGAGTGGTCTTTCCACTGCTACTG; Rev, CCCCAATTTTGCCTCTGGCTGGCTTT); SNP_A-2034029 (rs11079830, HOXB6) bis-For, TTTAGGTGTGGTGTTTAAAAGAATGT; bis-Rev, CAAATTAAAATTTCCCCAAAAAAA (unconverted sequences For, CCTAGGTGTGGTGTCCAAAAGAATGC; Rev, CAGATTGGGGTTTCCCCAAAAAGA). The PCR products were cloned using the TopoTA Cloning System (Invitrogen) and the resulting plasmids were sequenced.

[^{3}H]dCTP incorporation assay. The cytosine extension assay was done using 0.5 μg DNA as previously described (22). A standard curve was established using fixed ratios of universal methylated and unmethylated DNA (Millipore). DNA was digested with 20 units of *Hpa*II for 18 h at 37°C. The cytosine extension reaction was done by adding 3 μL of 10× PCR buffer II, 0.8 μL of $MgCl_2$, 0.75 unit of AmpliTaq DNA polymerase (Applied Biosystems, Inc.), and 0.15 μL of [^{3}H]dCTP (57.4 Ci/mmol; Perkin-Elmer) to the digested product and incubated at 56°C for 1 h. Samples were applied to DE-81 ion-exchange filters and washed thrice with 0.5 mol/L Na-phosphate buffer. After air-drying, the filters were processed for scintillation counting. The [^{3}H]dCTP incorporation into DNA was expressed as mean disintegration per minute per microgram of DNA. Assuming a linear relationship between disintegration per minute and percent methylation (22), the degree of methylation in the samples was estimated based on measurements of fixed ratios of control methylated and unmethylated DNA.

Antibodies and immunohistochemistry. For detecting nuclear 5-methyl-C in formalin-fixed paraffin-embedded and frozen tissue sections, we used a mouse monoclonal antibody, 5-methylcytosine (Ab-1; Calbiochem), which has previously been validated for this purpose (23, 24). Antigen retrieval in formalin-fixed paraffin-embedded sections was by microwave heating for 7 min at the high setting (bringing the solution to a boil) followed by 7 min at the low setting (during which the solution was maintained at a gentle boil) in 1× TBS with 0.1% Tween 20 (TBS-T) containing 1 mol/L sodium citrate. After antigen retrieval, the formalin-fixed paraffin-embedded sections were exposed to 3.5 N HCl for 15 min at room temperature and washed in TBS-T. Subsequently sections were treated with 0.3% peroxidase to quench endogenous peroxidase activity and were incubated with 5% normal horse serum for 30 min followed by overnight incubation with the anti–5-methyl-C monoclonal antibody at 1:1,000 dilution at room temperature. The majority of slides contained both cancerous and normal tissues, but when such a slide was not available, both control and cancer slides were treated identically. For detection of ASMA and DNA methyltransferase (DNMT; both antibodies from Abcam), the same antigen retrieval procedure was used. Slides were not exposed to HCl and a rabbit polyclonal antibody was used at 1:100 dilution. Antibody detection was done by incubation with biotinylated goat anti-mouse and anti-rabbit secondary antibodies (DAKO) at 1:200 dilution for 30 min at room temperature. Slides were developed for 30 s to 1 min using the 3,3′-diaminobenzidine staining kit (DAKO) and were counterstained with hematoxylin. For dual staining of 5-methyl-C and ASMA, the above procedure was followed for the anti–5-methyl-C staining, and subsequently, slides were incubated with the ASMA antibody and developed with the 5-bromo-4-chloro-3-indolyl phosphate/nitroblue tetrazolium alkaline-phosphatase substrate kit (Vector Labs). Frozen sections were fixed in acetone and were not subjected to antigen retrieval. Sections were exposed to 3 N HCl for 10 min at room temperature and washed in PBS. Simultaneous incubations with both primary antibodies at 1:1,000 dilution for anti–5-methyl-C and 1:100 dilution for anti-αSMA were overnight at 4°C in PBS containing 5% bovine serum albumin and 3% normal horse serum. Subsequently, secondary antibodies (Texas red–labeled donkey anti-goat and FITC-labeled donkey anti-rabbit) at 1:300 dilution were used for detection (Jackson ImmunoResearch Laboratories). The intensity of nuclear staining was measured using the ImageJ software (ImageJ v 1.38) after outlining the nuclear area of ASMA-positive intraepithelial cells.

Quantitative real-time reverse transcription-PCR. Quantitative real-time reverse transcription-PCR was done using a 7300 Fast Real-Time PCR System (Applied Biosystems). Reactions were done in triplicate in 96-well optical reaction plates. Each reaction contained cDNA reverse transcribed from 5 ng total RNA, 1× Power SYBR Green PCR master mix (Applied Biosystems.), and 0.2 μmol/L of each specific primer pair, which were designed using online D-Lux software (Invitrogen) or Primer Express 3.0 software (Applied Biosystems) with at least one primer spanning two exons (*DNMT1*, F: TTCAAATTCTGTGTGAGCTGTGC, R: cgggtGTGGCTGAGTAGTAGAGGACCcG; *DNMT3a*, F: ATTGATGAGCGCACAAGAGAGC, R: cggaaGCAGATGTCCTCAATGTTCcG; *DNMT3b*, F: AATGTTGTAGCCATGAAGGTTGG, R: cggttGGATTACACTCCAGGAACcG; *HPRT1*, TTATGGACAGGACTGAACGTCTTG, R: CCAGCAGGTCAGCAAAGAATT). The thermal cycling conditions were as follows: 50°C for 2 min, 95°C for 10 min, followed by 40 cycles of 15 s at 95°C for denaturation and 1 min at 60°C for annealing and extension. The relative expression level of a target gene in a particular sample is calculated as $2^{-\Delta\Delta CT}$, where $\Delta\Delta C_T = \Delta C_{T(sample)} - \Delta C_{T(calibrator)}$ (ref. 23).

Results

MSNP analysis of DNA from early-passage cancer-associated myofibroblasts. Using the MSNP procedure, we analyzed genomic

[9] http://biosun1.harvard.edu/complab/dchip/
[10] http://www.urogene.org/methprimer/

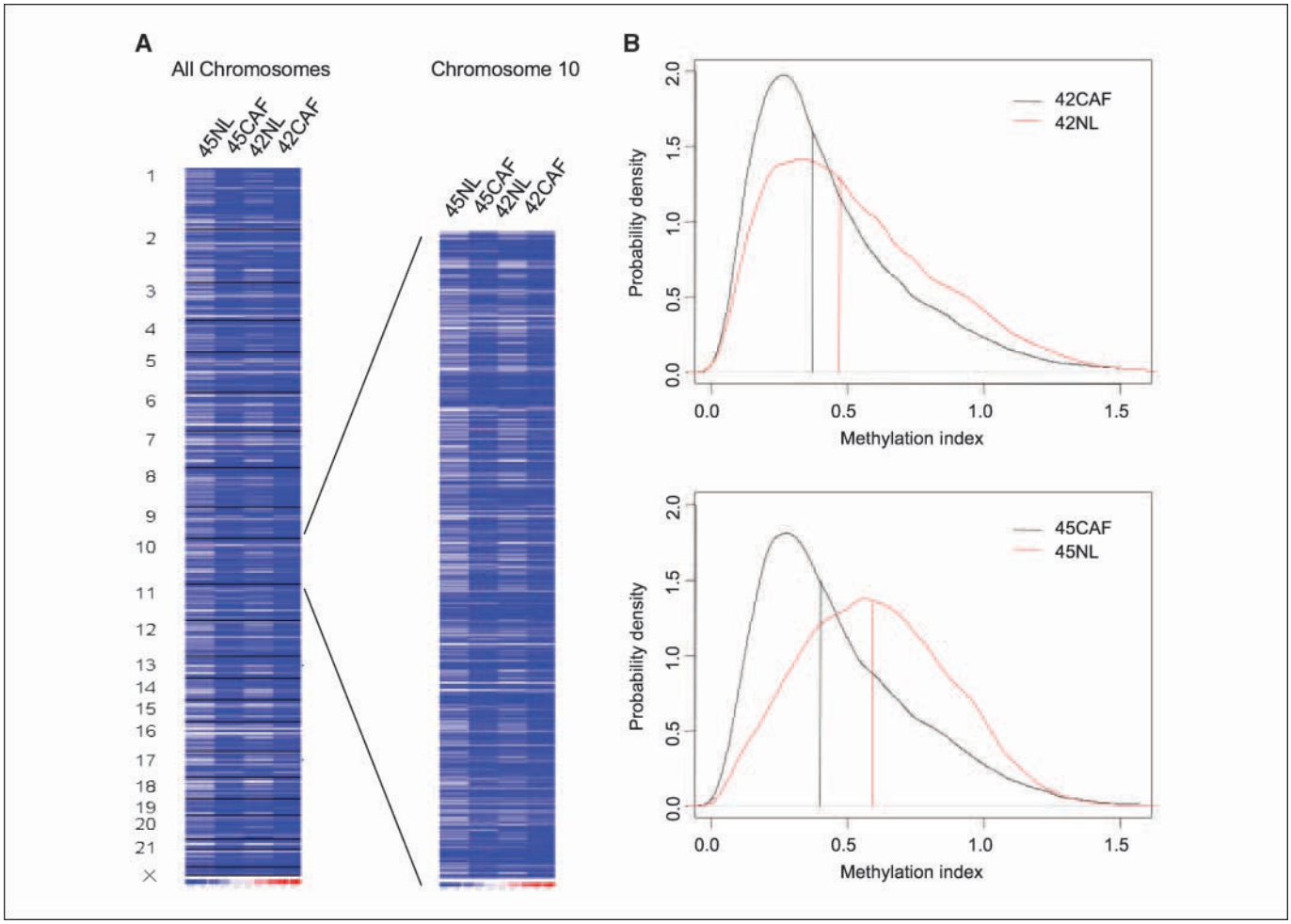

Figure 1. MSNP data showing loss of DNA methylation in cancer-associated myofibroblasts. *A,* methylation index values for class 2 SNPs (Affymetrix 250K StyI arrays) displayed by physical position along the human chromosomes (*left*) and zoomed in to chromosome 10 (*right*). In each of the two cases examined (case 45 and case 42), the MSNP analysis was a comparison of early-passage myofibroblasts isolated from within the polypoid intestinal-type carcinoma [cancer-associated fibroblasts (*CAF*)] to normal control myofibroblasts isolated from gastric tissue 10 cm away from the carcinoma (*NL*). Loss of methylation (*darker blue color*) is seen uniformly across all chromosomes, and the zoomed-in region is one example. *B,* histograms of methylation index for class 2 SNPs in the two cases. Both cases show a shift in the distribution to lower values in the cancer-associated myofibroblasts, with this loss being most severe in case 45. *Vertical lines,* median methylation index for each sample.

DNA from early-passage (p3–4) myofibroblast cultures prepared from gastrectomy specimens from two patients with intestinal-type gastric carcinomas. For each patient, we compared the pattern of DNA methylation in myofibroblasts isolated from within the tumor (cancer-associated myofibroblasts) to the pattern of methylation in myofibroblasts isolated from gastric tissue of the same specimen 10 cm away from the tumor at the negative surgical margin (control myofibroblasts). Because most patients with gastric cancers have underlying abnormalities of chronic gastritis, the tumor-distant myofibroblasts cannot be considered completely normal. Nonetheless, these cells from the same organ of the same individual are the closest matched control for this type of experiment, in which we sought to uncover epigenetic abnormalities in the tumor stroma. The MSNP data were from duplicate technical replicates with *Sty*I alone (*S*) and *Sty*I + *Hpa*II (*SH*) and a single determination with *Sty*I + *Msp*I (*SM*) for each of the DNA samples.

First, using the MSNP data from the *S* genomic representations, we asked whether there were detectable abnormalities of DNA copy number specific to the tumor-associated myofibroblasts. Setting the numerical ploidy as 2 in the tumor-distant myofibroblasts and processing the data by the standard approach of normalization, model-based expression, and chromosome analysis in dChip, no chromosomal or subchromosomal aneuploidies were seen in the tumor-associated fibroblasts. To examine DNA methylation, we next compared the signal intensities in the *S* versus *SH* genomic representations at informative SNP-tagged loci (class 2 SNPs; ref. 18), bioinformatically defined as those SNPs on the array that are within *Sty*I restriction fragments that contain internal *Hpa*II sites. To select the most technically reliable markers, for a class 2 SNP-tagged locus to be brought forward in the analysis, we additionally required that the average intensity in *SM* was reduced by >70% compared with the average with *S*. To facilitate a numerical analysis for losses and gains of DNA methylation, we next calculated a methylation index for each class 2 *Sty*I fragment, first subtracting the mean value for the *SM* representations as background and then using the formula $(SH_{av} - S_{av})/(S_{av}) + 1$, which yields a value near zero for an unmethylated locus and a value near 1 for a methylated locus. We

imported the resulting values to dChip and displayed these methylation index values by chromosome position. As shown visually and numerically in Fig. 1*A* and *B*, this procedure indicated that in both patients the tumor-associated myofibroblast DNA was hypomethylated on average at *Hpa*II sites adjacent to the class 2 SNPs queried by these arrays, compared with the DNA isolated from the control myofibroblasts distant from the tumors. This loss of methylation was more severe in case 45, but the phenomenon was also seen in case 42.

Validation and extension of the MSNP data by bisulfite sequencing and [^{3}H]dCTP incorporation assay. To search for loci with recurrent loss of methylation, and to ask whether any loci queried by the array might have undergone the opposite phenomenon of gain of methylation, we first eliminated those class 2 loci that did not vary substantially in methylation index across the four biological samples and then subjected the methylation index values for the remaining class 2 loci to supervised hierarchical clustering. This procedure identified a substantial group of loci with consistent loss of methylation and a much smaller group with consistent gain of methylation. We chose two of these loci, one with loss of methylation and one with gain of methylation reported by MSNP, for independent validations using a standard procedure of bisulfite conversion followed by PCR, cloning, and sequencing. This procedure scores methylation not only at *Hpa*II sites but also at all CpG dinucleotides between the PCR primers. As shown in Fig. 2, the bisulfite sequencing results matched the direction of the changes seen in the MSNP data, and the altered methylation affected multiple CpG sites in addition to the *Hpa*II sites.

To independently confirm the global hypomethylation reported by MSNP, we used a cytosine extension assay that has previously been validated for assessing global genomic 5-methyl-C (22). This assay measures the incorporation of [^{3}H]dCTP in a fill-in reaction on CG overhangs in *Hpa*II-digested genomic DNA. As shown by the standard curve and experimental results in Fig. 3, there was a significant decrease in methylation content in both of the cancer-associated myofibroblast samples that had been subjected to MSNP analysis, as compared with the tumor-distant myofibroblast control samples. We also performed this global methylation assay on genomic DNA from three additional cases of matched cancer-associated and control myofibroblast preparations and found a similar decrease in 5-methyl-C content in all cases (Fig. 3*B*). To also assess the effect of prolonged passaging in culture on 5-methyl-C content, we isolated DNA from myofibroblasts comparing the results at three versus six passages. As predicted from the prior literature (24), we observed a decrease in 5-methyl-C content in the later-passage cells, but the difference between the control and cancer-associated myofibroblasts was preserved at early and late passages (Supplementary Fig. S1).

Anti–5-methyl-C immunohistochemistry showing loss of DNA methylation in stromal myofibroblasts of primary gastric carcinomas. As noted above, it is well documented that patterns of DNA methylation can change as an artifact of tissue culture and increasing cell passage (24, 25). Thus, although we carried out our MSNP analysis on early-passage primary cultures, it was still important to verify that the widespread loss of CpG methylation observed in these samples accurately reflected the true situation in primary gastric cancers. To analyze a large series of cases, we

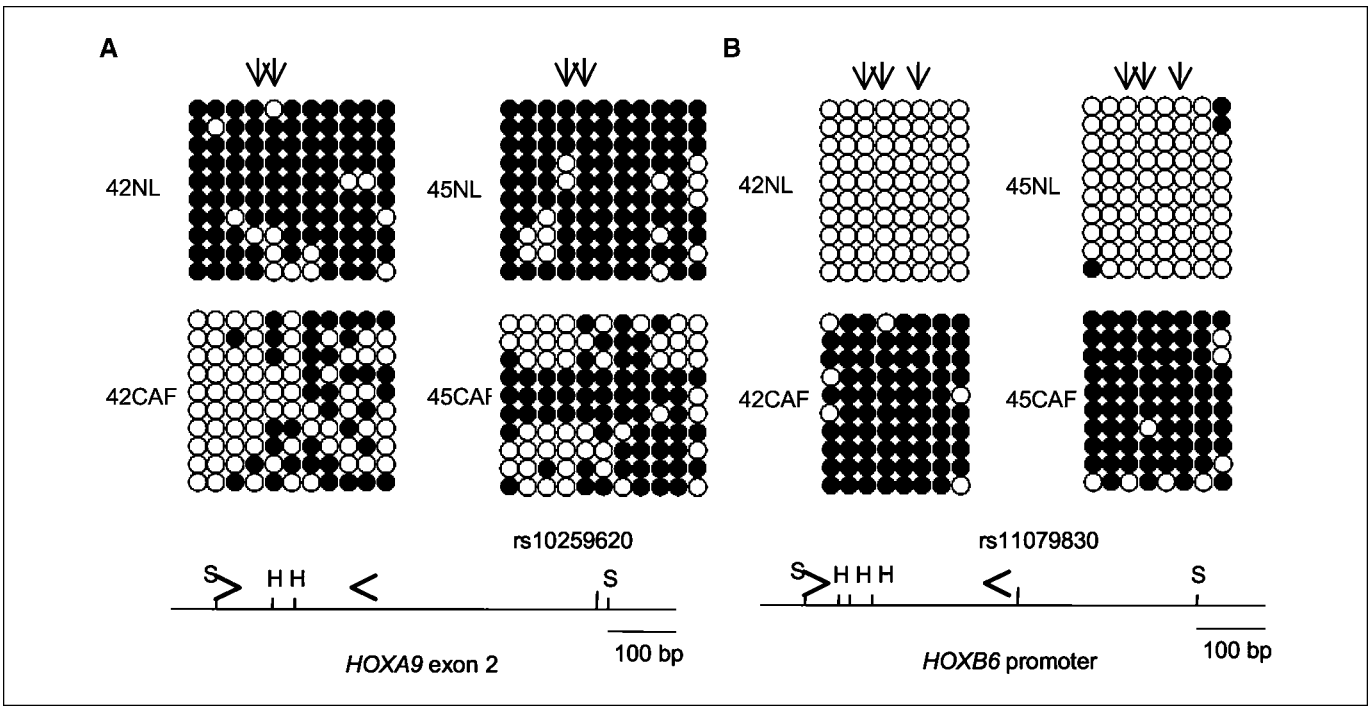

Figure 2. Validation of the MSNP data by bisulfite sequencing. *A,* bisulfite sequencing of one of the many SNP-tagged loci that showed a reduced methylation index in cancer-associated myofibroblasts from both cases: SNP ID rs10259620; in *HOXA9* exon 2. Genomic DNA was bisulfite treated and then amplified by PCR using primers specific for the converted sequence. The bisulfite PCR products were cloned and multiple clones sequenced (*rows*). There are a larger number of unmethylated CpG dinucleotides (*white circles*) in the cancer-associated myofibroblasts (*CAF*) compared with the myofibroblasts distant from the tumors (*NL*). *B,* results for one of the few SNP-tagged loci (SNP ID rs11079830, *HOXB6* proximal promoter region) that showed an increased methylation index in both cases. There are a larger number of methylated CpG dinucleotides (*black circles*) in the cancer-associated myofibroblasts. *Vertical arrows,* the CpG dinucleotides in *Hpa*II sites between the PCR primers. Symbols in the restriction maps: *S, Sty*I; *H, Hpa*II; *horizontal arrows,* bisulfite PCR primers.

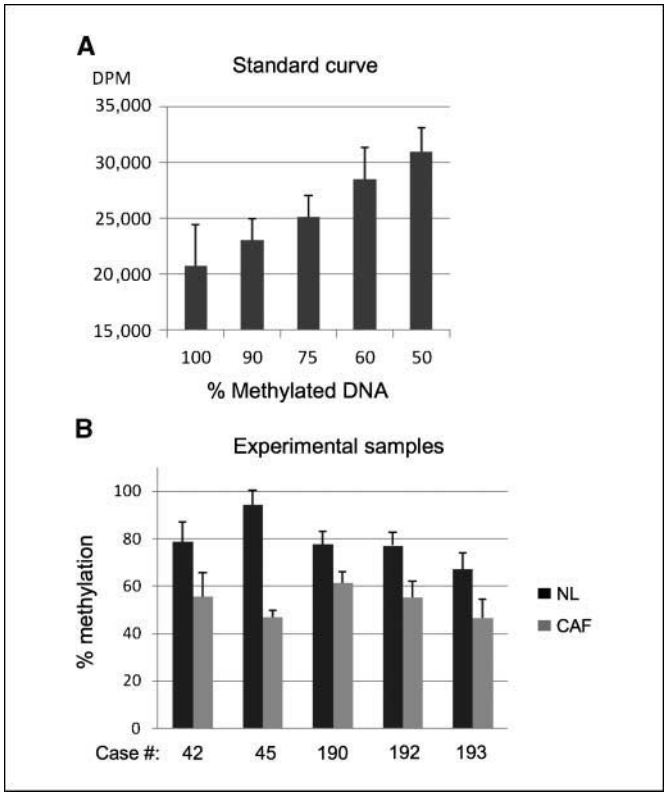

Figure 3. Validation of DNA hypomethylation in cancer-associated myofibroblasts by a [^{3}H]dCTP incorporation assay. *A,* calibration data from a mixing experiment with *in vitro* methylated and unmethylated human DNAs validating the ability of this assay to quantitate the average CpG methylation of genomic *Hpa*II sites. *DPM,* disintegration per minute. *B,* results with genomic DNA from the early-passage gastric myofibroblasts in five cases (#42 and #45 are cases represented in the MSNP data whereas the others are additional cases). There is consistent loss of methylation in the cancer-associated myofibroblasts (*CAF*) compared with myofibroblasts from noncancerous gastric mucosa (*NL*) in all cases, albeit with some variability in the extent of loss from case to case. *Columns,* mean of triplicate determinations; *bars,* SD.

used immunohistochemistry on archival formalin-fixed paraffin-embedded tissues, detecting nuclear 5-methyl-C with a monoclonal antibody that has been well characterized in previous studies of global loss of DNA methylation in the malignant epithelial component of several types of carcinomas in humans (26–29). First considering the normal controls for this analysis, while the precise identity of the normal precursors of cancer-associated myofibroblasts is not yet known, we observed strong nuclear staining with anti–5-methyl-C both in intraepithelial ASMA-positive spindle cells not associated with blood vessels (intraepithelial myofibroblasts) and in myofibroblasts of the thin muscularis mucosae layer immediately under the normal epithelium. As previously described, we noted a loss of anti–5-methyl-C staining in the malignant epithelial cells of the majority of the diffuse and intestinal-type gastric cancers (Figs. 4 and 5; Supplementary Table S1). For the formalin-fixed paraffin-embedded analyses, we identified ASMA-positive cells by alternating anti-ASMA and anti–5-methyl-C in serial sections. This parallel staining revealed an obvious loss of anti–5-methyl-C staining in the ASMA-positive myofibroblast cells in a majority of the cancer specimens (Fig. 4). Tumor-infiltrating lymphocytes did not exhibit a loss of staining and, hence, served as internal controls (Fig. 4). Qualitative scoring of the anti–5-methyl-C immunohistochemistry in the series of 10 intestinal-type and 6 diffuse-type gastric cancers revealed a consistent relative loss of staining intensity in the cancer-associated myofibroblasts in every case, albeit with some variation in the extent of this loss, as listed in Supplementary Table S1.

To verify the difference in staining intensity in rigorously defined myofibroblasts, we also performed dual ASMA and anti–5-methyl-C staining on the same histologic section for several of these cases, using two-color immunohistochemistry on formalin-fixed paraffin-embedded sections and dual-color immunofluorescence on frozen sections. As shown by the examples in Fig. 5, by dual-color immunohistochemistry, we confirmed the reduction in nuclear staining intensity for 5-methyl-C in cells in ASMA-positive cancer-associated myofibroblasts, relative to ASMA-positive non–cancer-associated myofibroblasts in two cases of intestinal-type and one case of diffuse-type gastric adenocarcinoma. As an important technical point, in these cases the use of blocks from the margin of the surgical resection allowed us to capture images of the cancer-associated and non–cancer-associated stroma from a single tissue section on a single slide. For quantitative assessment of these findings, we used dual-color immunofluorescence to examine frozen sections of the same two intestinal-type gastric cancer cases. As shown in Fig. 5*B* and *C*, this procedure confirmed the loss of nuclear 5-methyl-C in the cancer-associated myofibroblasts.

To begin to address whether the changes in methylation content are cancer specific or, alternatively, are due to nonspecific stromal cell proliferation, as can occur in various reactive conditions, we carried out immunohistochemistry for nuclear 5-methyl-C in four partial gastrectomy specimens containing benign gastric ulcers. As shown by the example in Supplementary Fig. S2, comparing reactive proliferating fibroblasts in the ulcer bed to comparable cells under the adjacent unaffected gastric mucosa, there was no change in 5-methyl-C staining of these reactive stromal cells in any of the four benign ulcers.

Global DNA hypomethylation in stromal myofibroblasts of dysplastic lesions in a mouse model of gastric carcinoma. To ask whether these findings could be extended to a well-controlled animal model system, we examined DNA methylation in a newly developed transgenic mouse model of gastric cancer in which an IL-1β cDNA is expressed from the gastrin promoter (17). This model is advantageous for studying tumor progression because low-grade dysplastic gastric lesions are observed by 6 to 9 months and progress to carcinoma *in situ* over the subsequent 6 to 8 months. When we carried out immunohistochemistry for 5-methyl-C on formalin-fixed paraffin-embedded sections of stomachs from these mice, we observed a striking loss of staining in reactive myofibroblasts already evident in the early dysplastic lesions, accompanied by a definite but somewhat less pronounced loss of 5-methyl-C immunostaining in the dysplastic epithelial cells (Fig. 6). As in the human cases, the infiltrating leukocytes maintained nuclear anti–5-methyl-C staining and served as a positive control for the immunohistochemistry procedure. At the more advanced stage of *in situ* carcinoma, both the malignant epithelial cells and the stromal myofibroblasts showed loss of nuclear 5-methyl-C (Fig. 6).

Lack of obvious changes in DNMT expression in cancer-associated myofibroblasts. DNMT1, DNMT3a, and DNMT3b are the DNMTs responsible for methylating cytosine in CpG dinucleotides. By quantitative PCR, we found no evidence for strongly altered expression of the mRNAs for these enzymes between the

cultured cancer-associated and control myofibroblasts (Supplementary Fig. S3). In our hands, the sensitivity of immunohistochemistry for detecting DNMT1 was not high enough to determine whether the amounts of this protein varied between the normal and cancer-associated myofibroblasts, as neither of these cells were detectably stained, whereas the malignant epithelial cells of the gastric carcinomas were often found to be strongly positive (Supplementary Fig. S3). Additional analysis with more sensitive antibody reagents, when available, will be necessary to definitively answer whether decreased expression of DNMTs plays a role in the global reduction of CpG methylation in cancer-associated myofibroblasts.

Discussion

Given the increasing evidence for a functional contribution of stromal myofibroblasts in the progression of human carcinomas, it is important to understand the genomic changes that accompany the conversion of normal myofibroblasts into cancer-associated myofibroblasts. Myofibroblasts are prominent elements of the tumor stroma in most types of human carcinomas, along with tumor-associated blood vessels and inflammatory cells. Their exact origin is an area of active research and candidate precursor cells include fibroblasts, smooth muscle cells, and bone marrow–derived stem cells (4). In the intestine, for example, myofibroblasts share several properties with the smooth muscle cells of the muscularis mucosae and seem to arise histologically from that layer (30); in the invasive gastric carcinomas (intestinal type) that we have examined, the histology also suggests that at least some of these cells have proliferated from this layer. In this study, we have defined myofibroblasts as spindle-shaped cells in the mucosa and muscularis mucosae that express αSMA and are not part of blood vessel walls. Smooth muscle cells of the muscularis propria are also SMA positive, but here we have specifically dealt with areas of the gastric cancers that had not invaded this deeper layer. Intraepithelial myofibroblasts are rare but detectable in normal noninflammed mucosa (16), and we have used both types of ASMA-positive cells (muscularis mucosae and intraepithelial) for comparison with cancer-associated myofibroblasts. It has been shown that their number (both the cellular thickness of the muscularis mucosae and the intraepithelial component) increases in preneoplastic tissue and in advanced cancer and that these cells come to constitute a significant portion of the tumor volume (31). Relevant to the controls in our study, myofibroblasts were originally described in nonmalignant wound healing and as such are also seen in gastric ulcers.

In a research area that is still evolving, recent studies have suggested that cancer-associated stromal cells undergo specific genetic and epigenetic changes. Our data shown here, from multiple modalities including MSNP for genomic methylation profiling, bisulfite sequencing, an *in vitro* radiolabeled cytosine incorporation assay, and anti–5-methyl-C immunohistochemistry on primary gastric cancers and dysplasias, together indicate that a major phenotypic change in cancer-associated myofibroblasts is a global reduction in DNA methylation. This phenomenon parallels the overall loss of DNA methylation that has been well documented in the malignant epithelial component of multiple types of human carcinomas (32–35), including gastric carcinomas (data shown

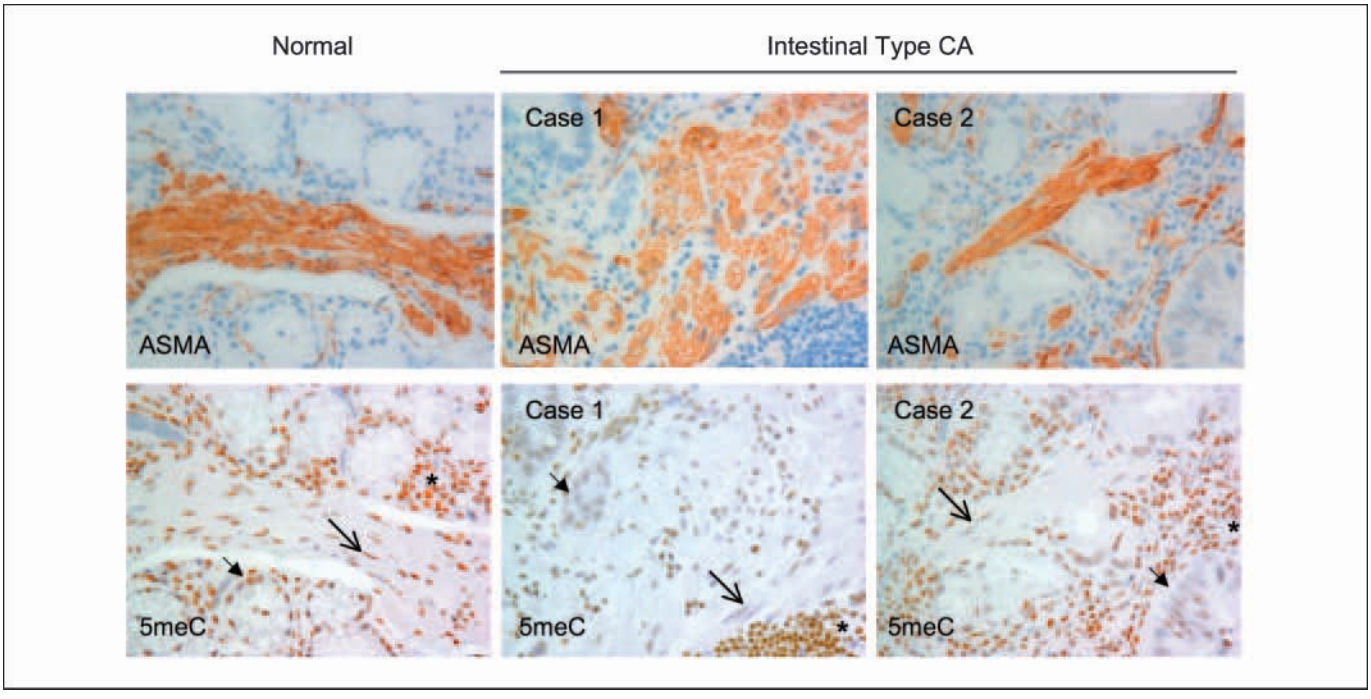

Figure 4. Anti–5-methyl-C immunohistochemistry showing loss of CpG methylation in myofibroblasts of primary gastric carcinomas. *Top* and *bottom,* immunohistochemistry with anti-ASMA and anti–5-methyl-C (*meC*), respectively. The control nonneoplastic gastric mucosa (*Normal*) was sampled at a location in the gastrectomy distant from an intestinal-type carcinoma. The ASMA-positive spindle-shaped myofibroblasts of the normal muscularis mucosae show strong nuclear staining with anti–5-methyl-C (*large arrow*), as do the normal epithelial cells (*small arrow*) and leukocytes (lymphocytes and polymorphonuclear cells; *asterisk*). The more rare ASMA-positive intraepithelial myofibroblasts also showed uniformly strong staining in multiple sections examined (example; *arrowhead*). Sections from within the cancers in two cases of intestinal-type gastric carcinomas (*CA*; *case 1* and *case 2*) show myofibroblasts (*large arrows*) and malignant epithelial cells (*small arrows*) with reduced immunohistochemistry intensity of 5-methyl-C. As in internal control, the anti–5-methyl-C staining of infiltrating leukocytes remains strong in the neoplastic tissue (*asterisks*).

here, and prior studies, e.g., refs. 36–38). However, the cause of genomic demethylation in cancer cells remains unresolved, and likewise, additional research will be needed to understand the mechanisms underlying this phenomenon in stromal myofibroblasts. Our data suggest that reduced expression of DNMTs probably does not explain this loss of methylation. Alternatively, it has been suggested that a deficiency in tissue or circulating methyl donors may contribute to demethylation in cancer.

A number of hypotheses have also been put forward about the downstream consequences of loss of CpG methylation in neoplastic epithelial cells, including effects on gene expression and genome stability. Our MSNP data for the two cases of short-term primary cultures of myofibroblasts isolated from within gastric cancers to cultures of myofibroblasts isolated from histologically uninvolved gastric mucosa distant from the cancers showed no evidence for genomic instability in terms of altered chromosomal or subchromosomal copy number and no evidence for LOH. It remains to be determined whether the cause and the consequence of global hypomethylation are distinct between the epithelial or neoplastic cell population and the cancer-associated stroma cells.

Emerging evidence suggests that expression of cytokines, proteolytic enzymes and their endogenous inhibitors (matrix metalloproteinases and tissue inhibitor of metalloproteinases), and growth factors are essential for the cross talk between cancer-associated myofibroblasts and malignant epithelial cells, including in gastric cancers (16, 39, 40). Several of these genes are up-regulated in cancer-associated myofibroblasts during the phenotypic change that accompanies a transformation from normal resting fibroblasts. Based on experiments in tissue culture with demethylating drugs, some of these genes have been suggested to be potentially up-regulated via hypomethylation (41). In general support of this observation is the finding that different patterns of gene expression are observed between cultured cancer-associated and non–cancer-associated myofibroblasts (30). In considering the functional correlates of global loss of methylation in these stromal cells, it is interesting that a recent study in a different organ system has found that decitabine treatment (inhibition of DNMTs) inhibits myofibroblast transdifferentiation from hepatic stellate cells (42). One of the most intriguing aspects of global hypomethylation in gastric cancer-associated myofibroblasts, shown by our analysis in the transgenic mouse model, is its occurrence early in cancer progression, at the dysplastic preinvasive stage. Thus, scoring this phenomenon by immunohistochemistry may prove useful in diagnosis of early gastric lesions.

Mechanistically, loss of DNA methylation may have several causes. For example, it could be a consequence of abnormal cellular proliferation, a local deficiency of methyl donors in dysplastic gastric mucosa, or both. Early studies have suggested that certain premalignant conditions may lead to decreased tissue folate content and, thus, a local deficiency in methyl donors (43). This same question has persisted for many years in the context of the parallel loss of methylation seen in malignant epithelial cells, and the answer

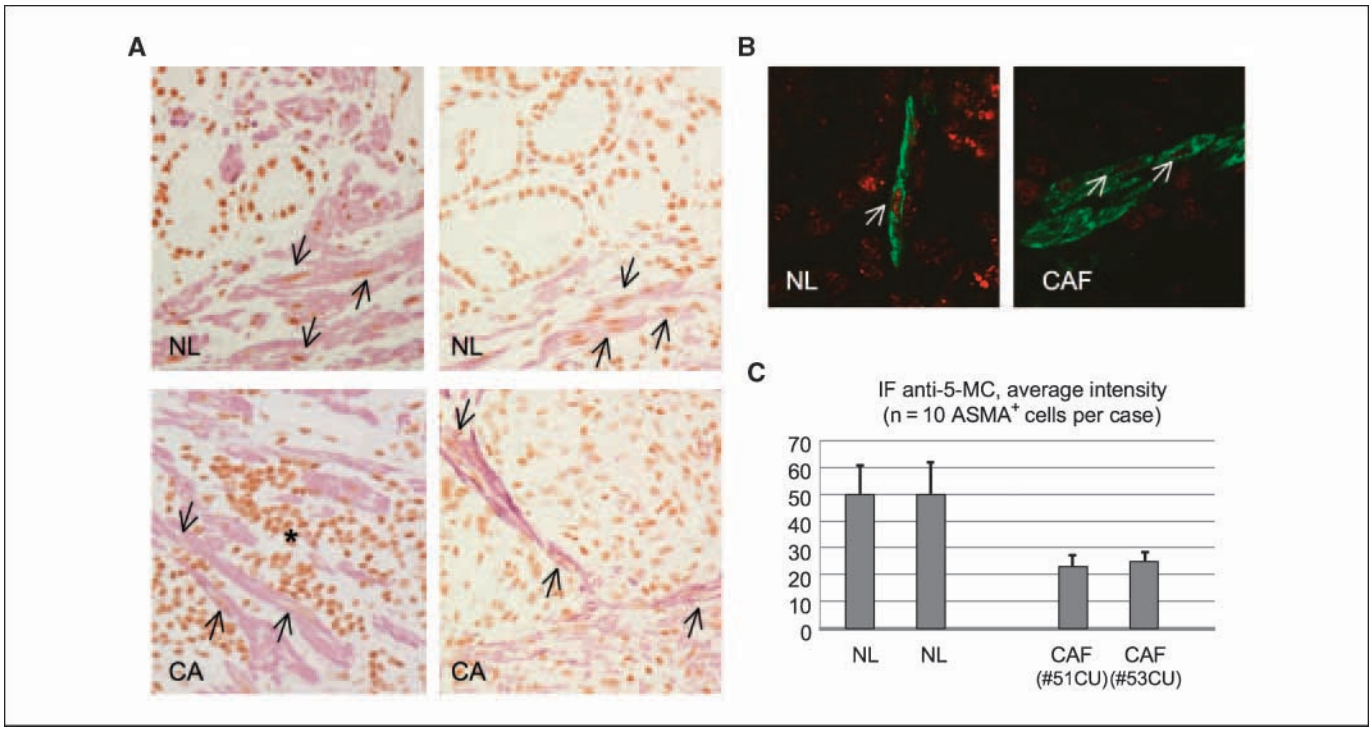

Figure 5. Dual staining to detect nuclear anti–5-methyl-C in ASMA-positive cells. *A,* dual-color immunohistochemistry [*brown,* anti–5-methyl-C (3,3′-diaminobenzidine); *blue,* anti-ASMA (nitroblue tetrazolium)] showing normal and tumor areas from cases of intestinal-type (*left*) and diffuse-type (*right*) gastric carcinoma. *Top,* mucosa at the uninvolved margin (*NL*); *bottom,* cancerous tissue (*CA*). There is an obvious reduction in nuclear 5-methyl-C immunostaining in the cancer-associated myofibroblasts (*arrows*), whereas the inflammatory cells surrounding the myofibroblasts have persistently high staining intensity (*asterisk*). *B,* dual-color immunofluorescence from another case of intestinal-type gastric cancer. *Left,* a confocal scanning microscopy image (100× objective) of nonneoplastic gastric mucosa (from negative surgical margin) showing an intraepithelial ASMA$^+$ (*green*) cell with strong anti–5-methyl-C staining (*red*) in the nucleus (*arrow*). *Right,* a group of intratumoral ASMA$^+$ cells in the intestinal-type gastric cancer from the same patient showing decreased nuclear anti–5-methl-C staining (*arrows*). *C,* quantitation of anti–5-methyl-C signal intensity from 10 individual ASMA$^+$ cells in two cases of gastric cancer and adjacent normal tissue. *IF,* immunofluorescence. In the intratumoral myofibroblasts from both cases, there is a global loss of DNA methylation.

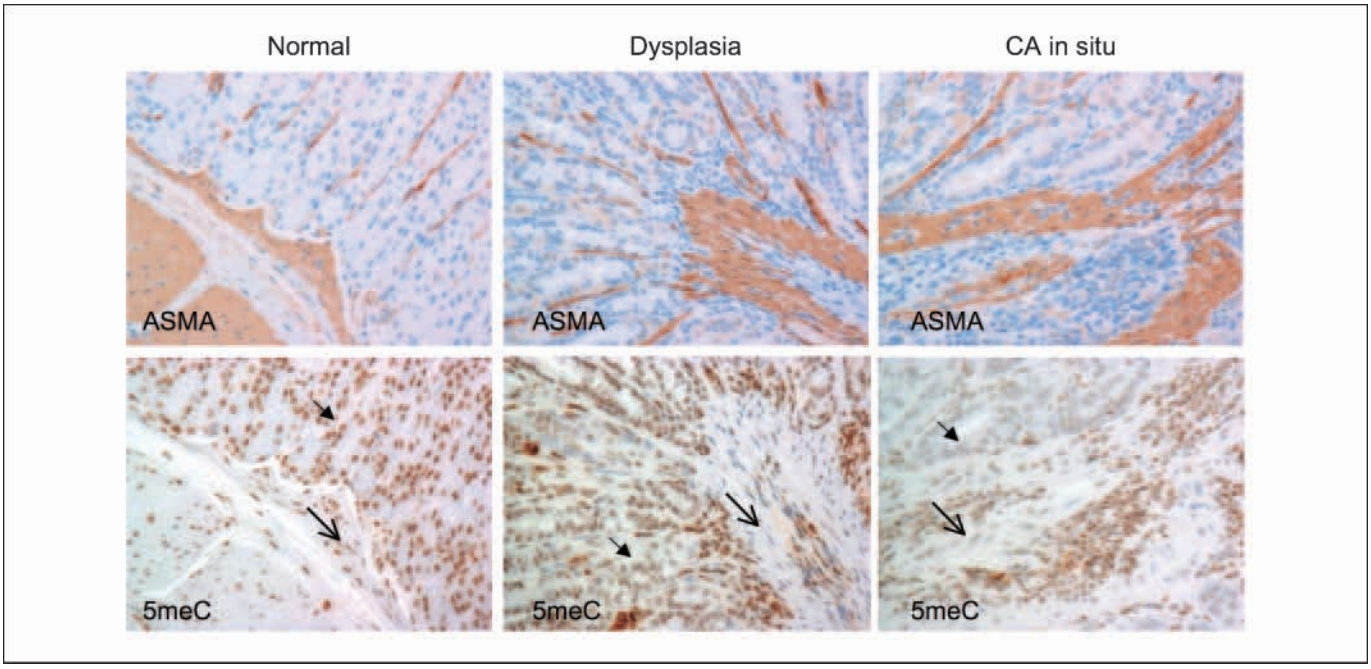

Figure 6. Change in anti–5-methyl-C staining of myofibroblasts in an IL-1β transgenic mouse model of progressive gastric dysplasia. Strong anti–5-methyl-C staining is seen for the epithelial cells (*small arrows*) and ASMA-positive myofibroblasts (*large arrows*) in histologically normal IL-1β transgenic gastric mucosa. There is an obvious decrease in anti–5-methyl-C staining in both epithelial and ASMA-positive cells in the dysplastic gastric mucosa and a persistent decrease in anti–5-methyl-C staining in epithelial and ASMA-positive cells in the carcinoma *in situ*. As an internal control, there is preserved anti–5-methyl-C staining of infiltrating lymphocytes in both the dysplasia and carcinoma *in situ*. These immunohistochemistry findings were consistent in each of two animals examined from each of the three categories (normal, dysplasia, and CA *in situ*).

may have ramifications for chemopreventive and therapeutic strategies that deliberately seek to increase or decrease cellular DNA methylation. Supplementation with methyl donors will need to be done taking into account the balance between reversing hypomethylation and potentially increasing tumor suppressor gene hypermethylation; thus, it will be important to define the time course of hypomethylation and hypermethylation in cancer initiation and progression, which may allow a more targeted approach to chemoprevention. If, as previously suggested (44), genomic hypomethylation is an early event that precedes at least some instances of gene specific hypermethylation, the optimal timing of methyl supplementation (i.e., folate, choline, betaine, selenomethionine, and *S*-adenosylmethionine) may be different from the optimal timing for administering methyltransferase inhibitors [i.e., (−)-epigallocatechin-3-gallate and decitabine]. This will be a challenging problem because pathologic gain of DNA methylation can occur very early in the tumorigenic pathway, sometimes as early as fetal organogenesis (35, 45, 46). More optimistically, our findings of reduced genomic methylation in cancer-associated stromal cells raise the possibility that demethylating drugs like decitabine might be able to exert anticancer activity or synergize with other anticancer agents in solid tumors not only via effects on the neoplastic cells but also possibly by provoking a hypomethylation crisis in the supporting stromal myofibroblasts.

Disclosure of Potential Conflicts of Interest

No potential conflicts of interest were disclosed.

Acknowledgments

Received 4/8/2008; revised 8/28/2008; accepted 9/1/2008.

Grant support: Medical Research Council and North West Cancer Research Fund (A. Varro) and grant U54-CA126513 (T.C. Wang and B. Tycko).

The costs of publication of this article were defrayed in part by the payment of page charges. This article must therefore be hereby marked *advertisement* in accordance with 18 U.S.C. Section 1734 solely to indicate this fact.

We thank Fuksz Zoltanne and Vesna Ilievski for technical assistance, and the editors for helpful suggestions on interpretation.

References

1. Dvorak HF. Tumors: wounds that do not heal. Similarities between tumor stroma generation and wound healing. N Engl J Med 1986;315:1650–9.
2. Tsujino T, Seshimo I, Yamamoto H, et al. Stromal myofibroblasts predict disease recurrence for colorectal cancer. Clin Cancer Res 2007;13:2082–90.
3. Orimo A, Weinberg RA. Stromal fibroblasts in cancer: a novel tumor-promoting cell type. Cell Cycle 2006;5:1597–601.
4. Desmouliere A, Guyot C, Gabbiani G. The stroma reaction myofibroblast: a key player in the control of tumor cell behavior. Int J Dev Biol 2004;48:509–17.
5. Mahadevan D, Von Hoff DD. Tumor-stroma interactions in pancreatic ductal adenocarcinoma. Mol Cancer Ther 2007;6:1186–97.
6. Chung LW, Baseman A, Assikis V, Zhau HE. Molecular insights into prostate cancer progression: the missing link of tumor microenvironment. J Urol 2005;173:10–20.
7. Fiegl H, Millinger S, Goebel G, et al. Breast cancer DNA methylation profiles in cancer cells and tumor stroma: association with HER-2/neu status in primary breast cancer. Cancer Res 2006;66:29–33.
8. Hu M, Yao J, Cai L, et al. Distinct epigenetic changes in the stromal cells of breast cancers. Nat Genet 2005;37:899–905.
9. Hanson JA, Gillespie JW, Grover A, et al. Gene promoter methylation in prostate tumor-associated stromal cells. J Natl Cancer Inst 2006;98:255–61.
10. Fukino K, Shen L, Matsumoto S, Morrison CD, Mutter GL, Eng C. Combined total genome loss of heterozygosity scan of breast cancer stroma and epithelium

reveals multiplicity of stromal targets. Cancer Res 2004; 64:7231–6.
11. Moinfar F, Man YG, Arnould L, Bratthauer GL, Ratschek M, Tavassoli FA. Concurrent and independent genetic alterations in the stromal and epithelial cells of mammary carcinoma: implications for tumorigenesis. Cancer Res 2000;60:2562–6.
12. Paterson RF, Ulbright TM, MacLennan GT, et al. Molecular genetic alterations in the laser-capture-microdissected stroma adjacent to bladder carcinoma. Cancer 2003;98:1830–6.
13. Walter K, Omura N, Hong SM, Griffith M, Goggins M. Pancreatic cancer associated fibroblasts display normal allelotypes. Cancer Biol Ther 2008;7:882–8.
14. Campbell IG, Qiu W, Polyak K, Haviv I. Breast-cancer stromal cells with TP53 mutations. N Engl J Med 2008; 358:1634–5; author reply 6.
15. Patocs A, Zhang L, Xu Y, et al. Breast-cancer stromal cells with TP53 mutations and nodal metastases. N Engl J Med 2007;357:2543–51.
16. McCaig C, Duval C, Hemers E, et al. The role of matrix metalloproteinase-7 in redefining the gastric microenvironment in response to *Helicobacter pylori*. Gastroenterology 2006;130:1754–63.
17. Tu SCG, Takaishi S, Bhagat G, et al. Overepression of IL-1β induced gastric inflammation and carcinoma through dysfunction of immunity and change of gastric microenvvironment in transgenic mice. Gastroenterology 2007;132:A–25.
18. Yuan E, Haghighi F, White S, et al. A single nucleotide polymorphism chip-based method for combined genetic and epigenetic profiling: validation in decitabine therapy and tumor/normal comparisons. Cancer Res 2006;66:3443–51.
19. Kerkel K, Spadola A, Yuan E, et al. Genomic surveys by methylation-sensitive SNP analysis identify sequence-dependent allele-specific DNA methylation. Nat Genet 2008;40:904–8.
20. Lin M, Wei LJ, Sellers WR, Lieberfarb M, Wong WH, Li C. dChipSNP: significance curve and clustering of SNP-array-based loss-of-heterozygosity data. Bioinformatics 2004;20:1233–40.
21. Li LC, Dahiya R. MethPrimer: designing primers for methylation PCRs. Bioinformatics 2002;18:1427–31.
22. Pogribny I, Yi P, James SJ. A sensitive new method for rapid detection of abnormal methylation patterns in global DNA and within CpG islands. Biochem Biophys Res Commun 1999;262:624–8.
23. Livak KJ, Schmittgen TD. Analysis of relative gene expression data using real-time quantitative PCR and the $2^{-\Delta\Delta CT}$ method. Methods 2001;25:402–8.
24. Wilson VL, Jones PA. DNA methylation decreases in aging but not in immortal cells. Science 1983;220: 1055–7.
25. Smiraglia DJ, Rush LJ, Fruhwald MC, et al. Excessive CpG island hypermethylation in cancer cell lines versus primary human malignancies. Hum Mol Genet 2001;10: 1413–9.
26. Piyathilake CJ, Frost AR, Bell WC, et al. Altered global methylation of DNA: an epigenetic difference in susceptibility for lung cancer is associated with its progression. Hum Pathol 2001;32:856–62.
27. Hernandez-Blazquez FJ, Habib M, Dumollard JM, et al. Evaluation of global DNA hypomethylation in human colon cancer tissues by immunohistochemistry and image analysis. Gut 2000;47:689–93.
28. Hinoi T, Akyol A, Theisen BK, et al. Mouse model of colonic adenoma-carcinoma progression based on somatic Apc inactivation. Cancer Res 2007;67:9721–30.
29. Piyathilake CJ, Johanning GL, Frost AR, et al. Immunohistochemical evaluation of global DNA methylation: comparison with *in vitro* radiolabeled methyl incorporation assay. Biotech Histochem 2000;75:251–8.
30. Powell DW, Adegboyega PA, Di Mari JF, Mifflin RC. Epithelial cells and their neighbors I. Role of intestinal myofibroblasts in development, repair, and cancer. Am J Physiol Gastrointest Liver Physiol 2005;289:G2–7.
31. Nakayama H, Enzan H, Miyazaki E, Toi M. α-Smooth muscle actin positive stromal cells in gastric carcinoma. J Clin Pathol 2002;55:741–4.
32. Gama-Sosa MA, Slagel VA, Trewyn RW, et al. The 5-methylcytosine content of DNA from human tumors. Nucleic Acids Res 1983;11:6883–94.
33. Feinberg AP, Vogelstein B. Hypomethylation distinguishes genes of some human cancers from their normal counterparts. Nature 1983;301:89–92.
34. Ehrlich M. DNA methylation in cancer: too much, but also too little. Oncogene 2002;21:5400–13.
35. Feinberg AP, Tycko B. The history of cancer epigenetics. Nat Rev Cancer 2004;4:143–53.
36. Kaneda A, Tsukamoto T, Takamura-Enya T, et al. Frequent hypomethylation in multiple promoter CpG islands is associated with global hypomethylation, but not with frequent promoter hypermethylation. Cancer Sci 2004;95:58–64.
37. Suzuki K, Suzuki I, Leodolter A, et al. Global DNA demethylation in gastrointestinal cancer is age dependent and precedes genomic damage. Cancer Cell 2006;9: 199–207.
38. Cravo M, Pinto R, Fidalgo P, et al. Global DNA hypomethylation occurs in the early stages of intestinal type gastric carcinoma. Gut 1996;39:434–8.
39. Crawford HC, Krishna US, Israel DA, Matrisian LM, Washington MK, Peek RM, Jr. *Helicobacter pylori* strain-selective induction of matrix metalloproteinase-7 *in vitro* and within gastric mucosa. Gastroenterology 2003;125:1125–36.
40. McDonnell S, Navre M, Coffey RJ, Jr., Matrisian LM. Expression and localization of the matrix metalloproteinase pump-1 (MMP-7) in human gastric and colon carcinomas. Mol Carcinog 1991;4:527–33.
41. Sato N, Maehara N, Su GH, Goggins M. Effects of 5-aza-2′-deoxycytidine on matrix metalloproteinase expression and pancreatic cancer cell invasiveness. J Natl Cancer Inst 2003;95:327–30.
42. Mann J, Oakley F, Akiboye F, Elsharkawy A, Thorne AW, Mann DA. Regulation of myofibroblast transdifferentiation by DNA methylation and MeCP2: implications for wound healing and fibrogenesis. Cell Death Differ 2007;14:275–85.
43. Kim YI, Fawaz K, Knox T, et al. Colonic mucosal concentrations of folate correlate well with blood measurements of folate status in persons with colorectal polyps. Am J Clin Nutr 1998;68:866–72.
44. Fraga MF, Herranz M, Espada J, et al. A mouse skin multistage carcinogenesis model reflects the aberrant DNA methylation patterns of human tumors. Cancer Res 2004;64:5527–34.
45. Moulton T, Crenshaw T, Hao Y, et al. Epigenetic lesions at the H19 locus in Wilms' tumour patients. Nat Genet 1994;7:440–7.
46. Yuan E, Li CM, Yamashiro DJ, et al. Genomic profiling maps loss of heterozygosity and defines the timing and stage dependence of epigenetic and genetic events in Wilms' tumors. Mol Cancer Res 2005;3:493–502.